# Resolution of Kirchhoff depth migration: offset and angle dependence

*J. Schleicher and L. T. Santos*

**email:** *js@ime.unicamp.br*

**keywords:** *Depth migration, resolution, angle-dependence*

**ABSTRACT**

*Amplitude anomalies imply strong amplitude variations over relatively short distances. Thus, a question fundamental to their quantitative interpretation asks for the influence of lower amplitudes on nearby higher amplitudes and vice versa, particularly in the context of post-migration AVO analysis. This question is directly related to the resolving power of seismic migration as a function of source-receiver offset. Horizontal resolution can be quantified in the time domain by means of the region around the migrated reflection point that is influenced by the migrated elementary wave. To obtain a numerical estimate for the mentioned zone of* horizontal influence *after migration, we investigate the migration output at a chosen depth point in the vicinity of the specular reflection point for a simple model of a horizontal interface with a vertical fault. We find that the region of influence before migration is well approximated by the projected Fresnel zone, where the half-period is replaced by an effective wavelet length. Spatial resolution after migration depends on the reflection angle rather than source-receiver offset. Thus, in principle, achievable resolution does not depend on reflector depth. As expected, migration improves the resolution for the usual seismic range of offsets. The achievable resolution remains almost the same for reflection angles up to about 30 degrees, but then strongly decreases. In consequence, a large-offset AVO/AVA analysis may lead to wrong results.*

## INTRODUCTION

Amplitude anomalies along a seismic reflector are a principal hydrocarbon indicator. An amplitude-variations-with-offset (AVO) analysis of the bright or dim spot can often increase the usefulness of these indicators. By their very nature, amplitude anomalies are spatially localized. Therefore, strong amplitude variations along the reflector occur at their boundaries, often over rather short distances. Due to the limited frequency content of the seismic waves, this means that the amplitudes within the anomaly are influenced by the different adjacent amplitudes. The ques-

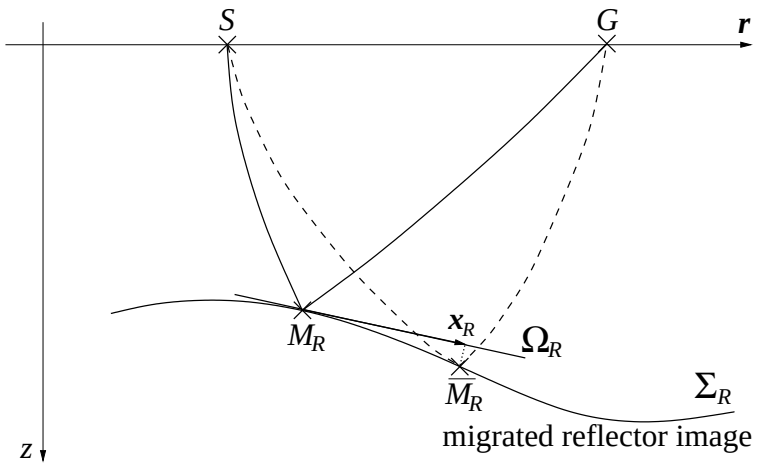


**Figure 1:** Horizontal resolution: influence of the migrated event at the specular reflection point $M_R$ on the migration result at the neighboring point $\overline{M}_R$ on the reflector.

tion of how much strong amplitude variations influence neighboring regions is directly related to horizontal resolution.

Seismic resolution after depth migration has been theoretically discussed by various authors (Berkhout, 1984; Beylkin, 1985a; Cohen et al., 1986; Bleistein, 1987). A recent comprehensive study on the subject was carried out in Vermeer (1999), where additional references on the subject can be found. When talking about horizontal resolution, a widely accepted notion among geophysicists is that "depth migration reduces the Fresnel zone." Although this is a very sloppy expression, because the Fresnel zone is a fixed-size frequency-dependent quantity associated with the reflected ray, we will see in this paper that there is a lot of truth in it. Firstly, horizontal resolution can indeed be quantified using a Fresnel zone concept. Secondly, for usual seismic reflection angles, seismic migration improves the horizontal resolution. It is, however, interesting to observe that for higher reflection angles, migration may actually worsen the horizontal resolution.

We find that horizontal resolution depends very much on the pulse stretch (see, e.g., Tygel et al., 1994) that is closely related to vertical resolution. Note that this implies to define resolution in a slightly different way from what is usually done in the literature. Conventionally, resolution is quantified by the minimal distance of two objects such that their images can still be recognized as two distinct ones. In this way, resolution is clearly a frequency-domain concept. For a more practical, time-domain concept, we need a different definition. Guided by the pulse distortion, we quantify horizontal resolution by means of the portion of the reflector around the specular reflection point $M_R$ that is influenced by the migrated elementary wave at $M_R$ (see Figure 1).

As shown in last year's report (Schleicher and Santos, 2000), the mentioned zone of "horizontal influence" after Kirchhoff migration, i.e., the region of reflector points $\overline{M}_R$that are influenced by the migration result at $M_R$, is the time-domain Fresnel zone. However, migration resolution is better than that. In this report, we study the improvement of resolution due to migration in a more quantitative way. In particular, we study the horizontal resolution of seismic migration

as a function of offset and angle. As shown by Tygel et al. (1994), the vertical resolution is the worse the greater the offset becomes. For a horizontal reflector below a constant-velocity overburden, it decreases proportionally to the cosine of the reflection angle. As we have seen last year, horizontal resolution qualitatively exhibits a similar behavior.

## FRESNEL ZONE

Seismic wave propagation in the high-frequency range is usually well-described by (zero-order) ray theory. For finite frequencies, however, a ray can only be viewed as a mathematical concept. In fact, there is a (frequency-dependent) spatial region in the vicinity of such a "mathematical ray" that influences the time-harmonic wavefield received at the end of the ray. Consequently a ray-theoretical investigation of the resolution of seismic methods must include a study of the extension of this region. By transferring concepts from physical optics (see, e.g., Sommerfeld, 1964), one can show that the main influence stems from the so-called *(first) Fresnel volume* of the ray, which is therfore often called the "physical ray". An excellent explanation of Fresnel volumes and their role in seismics is given in Hagedoorn (1954). Any cross-cut of the Fresnel volume by an (arbitrarily curved) surface intersecting the ray (not necessarily an interface in the medium) is called a *(first) Fresnel zone* at that surface (Sheriff, 1980; Gelchinsky, 1985; Knapp, 1991, see also references there).

### Time-domain Fresnel zone

In the frequency domain, the first Fresnel zone is defined as follows. A point $M$ is said to be inside the Fresnel zone pertaining to a certain point $P$ on the specular ray if the scattering contributions from $M$ constructively interfere with the monofrequency wavefield at the receiver. Physically, this is expressed by the condition that the lengths of the rays to and from $M$ must not differ by more than half a wavelength from the length of the specular ray. Mathematically, this condition translates to

$$|\tau - \tau_0| \leq T/2 \; , \tag{1}$$

where $T$ is the period of the monofrequency wave.

For an equivalent definition of the concept of a Fresnel zone in the time domain, the period $T$ in equation (1) must be replaced by some effective wavelet length $\tau_\varepsilon$ of the source pulse under consideration. Then, in the time domain, the above equation reads

$$|\tau - \tau_0| \leq \tau_\varepsilon \; . \tag{2}$$

Hubral et al. (1992) proposed to use the total theoretical wavelet length $\tau_t$ for $\tau_\varepsilon$. However, even for theoretical pulses like the Ricker wavelet where the pulse length exactly known, this turns out not to be a good measure for the actual pulse length. To find a better one in the framework of horizontal resolution, we have tested numerically several possible definitions for the effective pulse length based on the concepts detailed below. They are indicated in Figure 2a for a Ricker wavelet with a theoretical wavelet length of $\tau_t$ =64 ms.

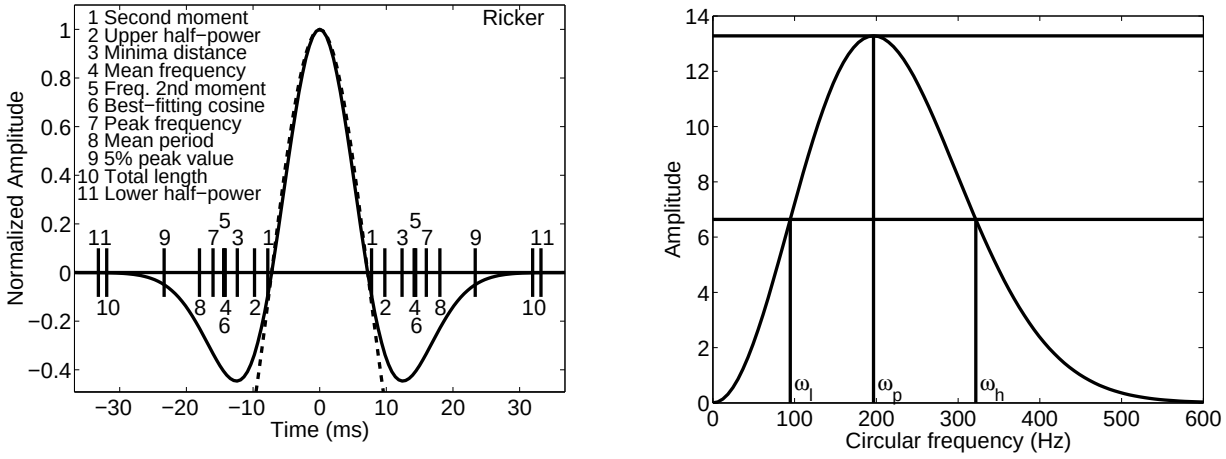


**Figure 2:** Left: Ricker wavelet with a theoretical wavelet length of $\tau_t = 64$ ms and its effective wavelet lengths. The dashed line is the cosine that best fits the main lobe, i.e., the cosine that has the same zeros as the wavelet. Right: Amplitude spectrum of the Ricker wavelet together with the upper and lower half-power frequencies $\omega_u$ and $\omega_l$ as well as the peak power frequency.

1. Time-domain second moment (Berkhout, 1982): $\tau_\varepsilon = 2\sqrt{M_2}$,
   where $M_2$ is the second moment of the wavelet, viz.,

$$M_2 = \frac{\int_{-\infty}^{\infty} (t - t_0)^2 f(t)^2 dt}{\int_{-\infty}^{\infty} f(t)^2 dt} \qquad \text{with} \qquad t_0 = \frac{\int_{-\infty}^{\infty} t f(t)^2 dt}{\int_{-\infty}^{\infty} f(t)^2 dt} \tag{3}$$

   being the center of the wavelet.

2. Upper half-power frequency: $\tau_\varepsilon = 2\pi/\omega_u$,
   where $\omega_u$ is the upper frequency where the power spectrum $|f(\omega)|$ has half its peak value (see Figure 2b).

3. Distance between minima: $\tau_\varepsilon = t_{m2} - t_{m1}$,
   where $t_{m1}$ and $t_{m2}$ are the positions of the (first) minima of the wavelet. Note that half this distance is also called the "tuning distance" of the (zero-phase) wavelet (Kallweit and Wood, 1982). For the Ricker wavelet, $t_{m2} - t_{m1} = \tau_t\sqrt{6}/2\pi$.

4. Mean frequency: $\tau_\varepsilon = 2\pi/\overline{\omega}$,
   where

$$\overline{\omega} = \frac{\int_{-\infty}^{\infty} \omega |f(\omega)| d\omega}{\int_{-\infty}^{\infty} |f(\omega)| d\omega} \; . \tag{4}$$

5. Frequency-domain second moment: $\tau_\varepsilon = 2\pi/\sqrt{\Omega_2}$,
   where
   $$\Omega_2 = \frac{\int_{-\infty}^{\infty} \omega^2 |f(\omega)|^2 d\omega}{\int_{-\infty}^{\infty} |f(\omega)|^2 d\omega} \tag{5}$$
   is the second moment of the wavelet in the frequency domain.

6. Best-fitting cosine or distance between zeros: $\tau_\varepsilon = 2\pi/\omega_c$,
   where $\omega_c$ is the frequency of the cosine that passes through zero at the same points as the wavelet. In other words, this wavelet length is the period of that monofrequency wave that best fits the actual wavelet. Thus, $\omega_c$ is the smallest frequency that satisfies $\cos\omega_c(t_{02} - t_{01}) = 0$, where $t_{01}$ and $t_{02}$ are the central zeros of the wavelet. Then, $\omega_c = \pi/(t_{02} - t_{01})$, and $\tau_\varepsilon = 2(t_{02} - t_{01})$. Note that half this distance is the half-period of $\cos\omega_c t$, which would be used in equation (1). For the Ricker wavelet, $(t_{02} - t_{01}) = \tau_t\sqrt{2}/2\pi$, where $\tau_t$ is the theoretical wavelet length.

7. Peak frequency $\tau_\varepsilon = 2\pi/\omega_p$,
   where $\omega_p$ is the frequency where the power spectrum $|f(\omega)|$ has its peak value (see Figure 2b). For the Ricker wavelet, $\omega_p = 4\pi/\tau_t$.

8. Mean period: $\tau_\varepsilon = \overline{T}$,
   where
   $$\overline{T} = \frac{\int_{-\infty}^{\infty} T(\omega)|f(\omega)|d\omega}{\int_{-\infty}^{\infty} |f(\omega)|d\omega} = \frac{\int_{-\infty}^{\infty} \frac{2\pi}{\omega}|f(\omega)|d\omega}{\int_{-\infty}^{\infty} |f(\omega)|d\omega}, \tag{6}$$
   is the mean period of the wavelet. In this integral, $T(\omega) = 2\pi/\omega$ is the period of the monofrequency wave with frequency $\omega$. Note that half this length is the mean half-period of the wavelet.

9. 5% of peak amplitude: $\tau_\varepsilon = t_{52} - t_{51}$,
   where $t_{51}$ and $t_{52}$ are the outermost points where amplitude of the wavelet falls below 5% of its peak value. This is a more practical measure of the wavelet length.

10. 0.1% of peak amplitude: $\tau_\varepsilon = t_{t2} - t_{t1}$,
    where $t_{t1}$ and $t_{t2}$ are the outermost points where amplitude of the wavelet falls below 0.1% of its peak value. For most practical wavelets, this length is equal to the total theoretical wavelet length $\tau_t$.

11. Lower half-power frequency: $\tau_\varepsilon = 2\pi/\omega_l$,
    where $\omega_l$ is the lower frequency where the power spectrum $|f(\omega)|$ has half its peak value (see Figure 2b).

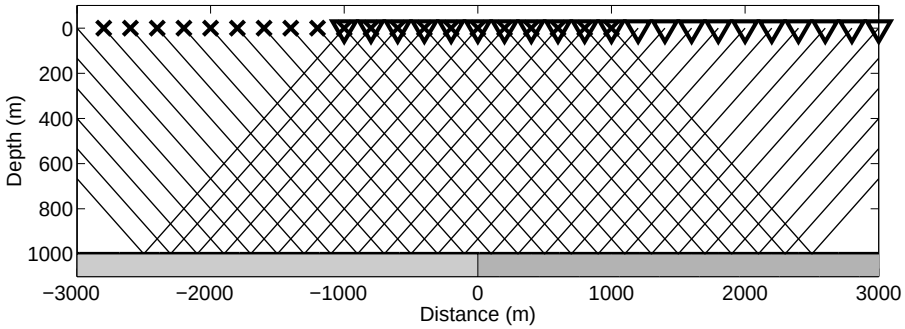


**Figure 3:** Earth model for a simple numerical experiment. Also shown is the ray family for a common-offset experiment with a source-receiver offset of 3000 m.

The effective wavelet lengths as determined by the various definitions in the above (increasing) order are indicated in Figure 2a by vertical bars. Figure 2b shows the power spectrum of the same Ricker wavelet. Also indicated are the peak power frequency $\omega_p$ as well as the upper and lower half-power frequencies $\omega_u$ and $\omega_l$. In view of equation (1), we have numerically tested not only the full effective wavelet lengths as defined above, but also the corresponding half lengths.

## NUMERICAL ANALYSIS

For the purpose of determining the best measure for the effective wavelet length in the context of horizontal resolution, and to demonstrate the lateral resolution of the seismic image before and after Kirchhoff depth migration, we have devised the following simple numerical experiment. Consider a horizontal interface below a homogeneous halfspace with an acoustic wave velocity of 6 km/s (see Figure 3). Below the interface, we consider a vertical fault at $x = 0$ km, separating two homogeneous blocks with velocities of 5 km/s and 5.5 km/s on the left and right side of the fault, respectively. In this model, we have simulated an ensemble of common-offset seismic surveys with source-receiver offsets ranging from 0 m to 7000 m. To avoid the influence of sampling and aperture on the final resolution, we have chosen midpoints at every 10 m from -5000 m to 5000 m. The reflection angle for the largest offset is about 74°.

### Resolution before migration

The model was chosen to demonstrate the influence of the fault on the seismic data. The simple fault model is ideal for this demonstration as it allows for a quantitative estimate of the transition zone between the two (constant) amplitudes on both sides of the fault. The numerical modeling was realized by an implementation of the 2.5-dimensional Kirchhoff integral. The source wavelet is a symmetrical Ricker wavelet with a duration of 64 ms.

The Kirchhoff data show how the information of the fault is distributed in the seismic amplitudes over a projected Fresnel zone. To make this even more evident, we have picked the peak amplitude along the seismic event. This amplitude was normalized so that the two constant amplitude values on both sides of the fault become minus one and one, respectively. The resulting normalized amplitude is shown in Figure 4 as a function of midpoint coordinate. We observe

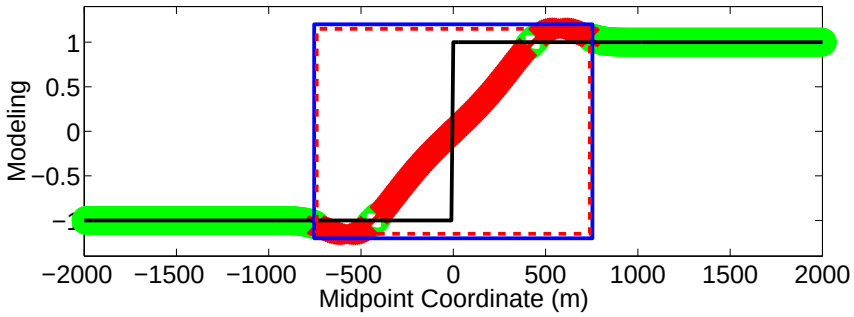


**Figure 4:** Normalized peak amplitude along the seismic reflection event. Also indicated are the boundaries of the time-domain projected Fresnel zone in the direction of the seismic line (solid box) and the estimate of the transition zone (dashed box).

that the abrupt horizontal velocity contrast leads to a smooth amplitude increase along the seismic reflection event across the fault. The estimated size of this transition zone (dashed box) is also indicated in Figure 4. To eliminate the influence of possible numerical errors, the transition was defined to end where the normalized amplitude differs by no more than 5% from the final value that is not affected by the fault.

Also indicated in Figure 4 are the boundaries of the time-domain projected Fresnel zone (solid box). For a common-offset experiment over a model with a horizontal reflector at depth $z$ below an overburden with a constant velocity $v$, the projected Fresnel zone is equal to the actual Fresnel zone, i.e., an ellipse with semi-axes $b = \sqrt{v\tau_\varepsilon z}$ and $a = b/\cos^{3/2}\theta$, where $\theta$ is the reflection angle. Indicated in Figure 4 is the size of the greater semi-axis $a$ that quantifies the extension of the Fresnel zone in the direction of the seismic line. The projected Fresnel zone in Figure 4 was calculated using for the effective wavelet length $\tau_\varepsilon$ the mean half-period, because this provides the best estimate. The transition zone coincides almost perfectly with the so predicted projected Fresnel zone.

The above experiment was repeated for all source-receiver offsets indicated above. Figure 5 shows the size of the estimated transition zone as a function of half-offset (plus signs), together with the predictions using the different definitions of the wavelet length. Indicated are the sizes of the projected Fresnel zone for entire (solid lines) and half wavelet lengths (dashed lines). The numbers correspond to those in Figure 2. Lengths number 5, 6, and 11 have been omitted since they are almost identical to number 4 and 10, respectively. The best prediction is achieved by the dashed curve number 8 (see also the zoom in the top left corner). This was calculated using half the mean period, which can also be interpreted as the mean half-period. This is a result that seems to be justified, given the definitions (1) and (2) of the Fresnel zones in the frequency and time domain, respectively.

Our first conclusion is that the effective wavelet length governs the horizontal resolution of seismic data before migration is the mean-half period.

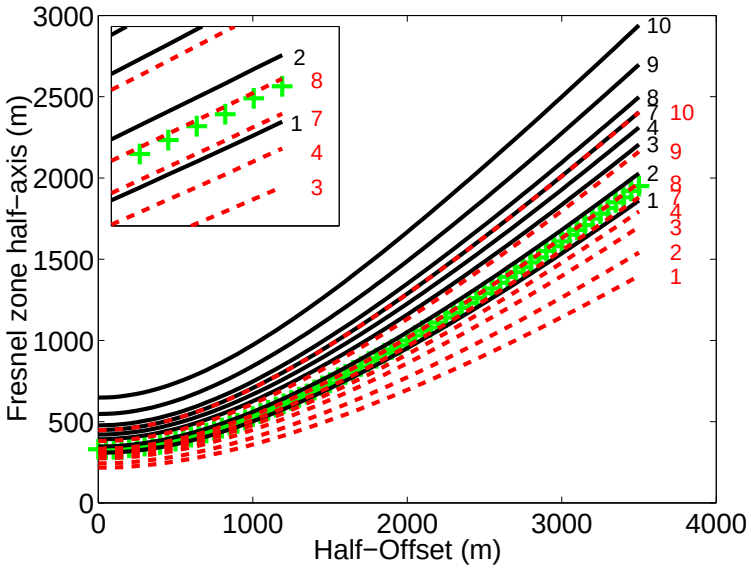


**Figure 5:** Half-axis of the transition zone of seismic data amplitudes across the vertical fault (plus signs). Also indicated are the predictions of the projected Fresnel zone using some of the different definitions of the effective wavelet length (solid lines) and the corresponding half lengths (dashed lines). Numbering is as before.

### Resolution after migration

A seismic prestack Kirchhoff depth migration. has been performed on all synthetic common-offset sections with source-receiver offsets between 0 m and 7000 m. After migration, the amplitude change from one side of the fault to the other has become much steeper than in the original data. This comes as no surprise since it is well-known that migration increases the lateral resolution. To better quantify this effect, Figure 6 shows the picked peak amplitudes along the migrated seismic event. In this figure, it is much easily appreciated that the change in amplitudes between the two values of the reflection coefficient at both sides of the fault is much more abrupt than in Figure 4. Our theoretical prediction for the size of the Fresnel zone, based on the results of

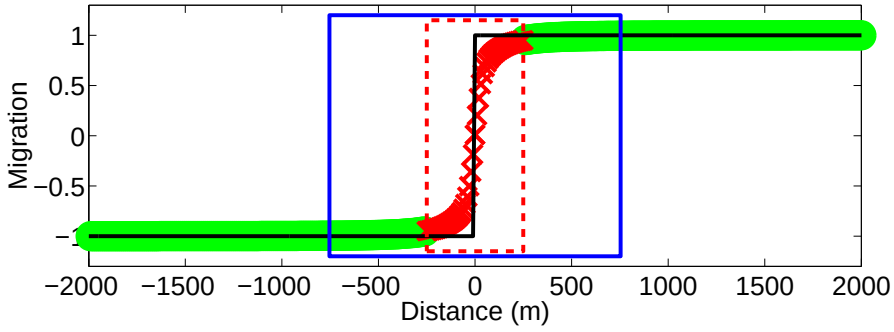


**Figure 6:** Normalized peak amplitudes of the migrated reflection event.

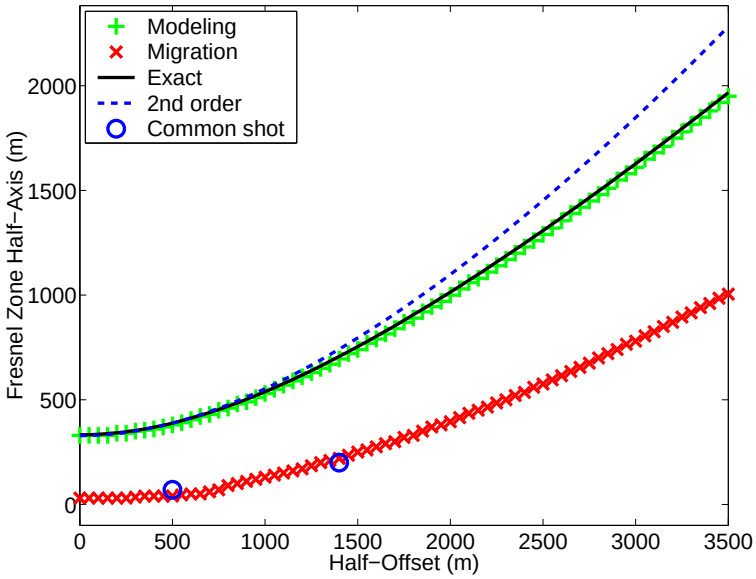


**Figure 7:** Half-axis of the residual transition zone before (plus signs) and after Kirchhoff depth migration (crosses). Also shown are the exact Fresnel zone and its paraxial (second-order) approximation, as well as the results of two common-shot experiments.

the previous section, is indicated by the solid box. The actual transition zone (dashed box) has been estimated in the same way as before. As expected, it has indeed been strongly reduced by Kirchhoff migration.

To put this investigation on a broader basis and make its results more conclusive, we have repeated this numerical comparison for source-receiver offsets between 0 m and 7000 m. Figure 7 shows the size of the estimated transition zones before (plus signs) and after migration (crosses) as a function of half-offset. We observe an improvement of resolution over the whole range of offsets. Also indicated are the estimated transition zones after migration of two common-shot datasets. They have been chosen such that the half-offset of the specular ray reflected at the fault is 500 m and 1400 m, respectively. Their values coincide quite well with the corresponding common-offset results. This suggests that the resolution after migration does not depend on the acquisition geometry, provided the aperture is sufficiently large. Common-shot migration needs a considerably larger aperture in order not to affect its resolution. It is, however, interesting to observe that, contrary to expectation, migration does not necessarily improve the seismic resolution. Figure 8 shows the results of the corresponding analysis for a reflector at a depth of 500 m. Under these circumstances the maximum reflection angle for the same offsets as before is 81°. For half-offsets beyond 2000 m, the transition zone is actually larger after migration than it was before.

To better understand the resolution achieved by Kirchhoff migration, we have investigated the transition zone as a function of the reflection angle $\theta$ (see Figure 9). Indicated are the sizes of the migrated transition zones for three different reflector depths. All three curves coincide almost perfectly. We immediately conclude from this figure that the horizontal resolution after migration actually depends on the reflection angle rather than on the source-receiver offset. In

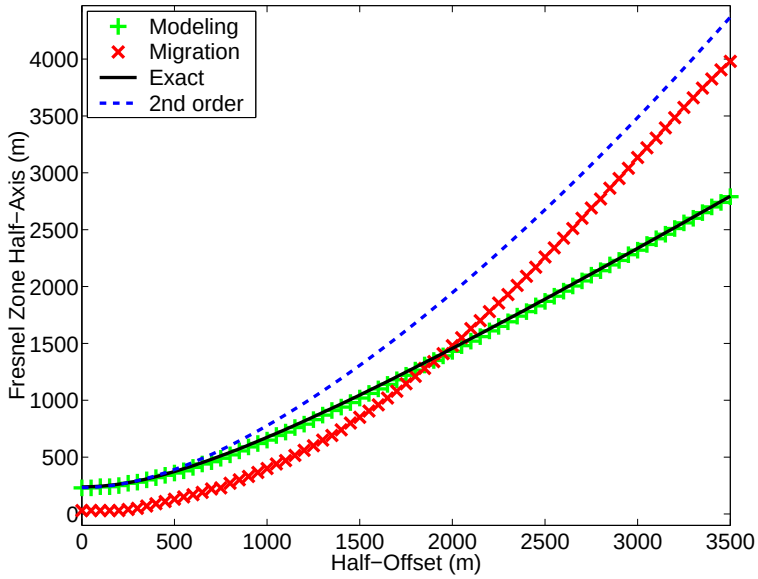


**Figure 8:** Half-axis of the residual transition zone before (plus signs) and after Kirchhoff depth migration (crosses) for a reflector at 500 m depth. Also shown are the exact Fresnel zone and its paraxial (second-order) approximation.

particular, it does not depend on the reflector depth. This is important to observe since it implies that deeper down reflectors can theoretically be imaged with the same resolution as shallower ones, provided the aperture is sufficiently large.

For a more quantitative understanding of the residual transition zone, we have tried to fit theoretical functions of the reflection angle to the data. Several functions, most of them with very odd exponents of sine and cosine functions, fit the data equally well. Only one of these curves presents exponents that seem to be theoretically explicable. It is given by

$$TZ(\theta) = A\frac{\sin\theta}{\cos^2\theta}\ , \tag{7}$$

where the proportionality factor has a value of $A \simeq 90$ m. Note, however, that this value is strongly dependent on the chosen definition of the transition zone. For a 3% criterion, we have already $A \simeq 115$ m. This curve described by equation (7) is indicated as a solid line in Figure 9. It fits the observed values reasonably well for reflection angles larger than about 20°. Below that value, the size of the transition zone remains almost constant at a value of $30$ m$\simeq v\tau_\varepsilon/4$, which is the value to be expected for zero offset and infinite aperture (Vermeer, 1999).

The offset dependence as described by the above formula, however, is in conflict with Vermeer's formula. This is probably due to the fact that Vermeer studies the resolution of two diffraction points at a short distance from each other rather than that of a reflector.

### Attempt of a geometric explanation

How can we understand the sine-over-cosine-square behavior of the horizontal resolution? For a possible explanation, consider Figure 10. We see the migrated reflector image symbolized by

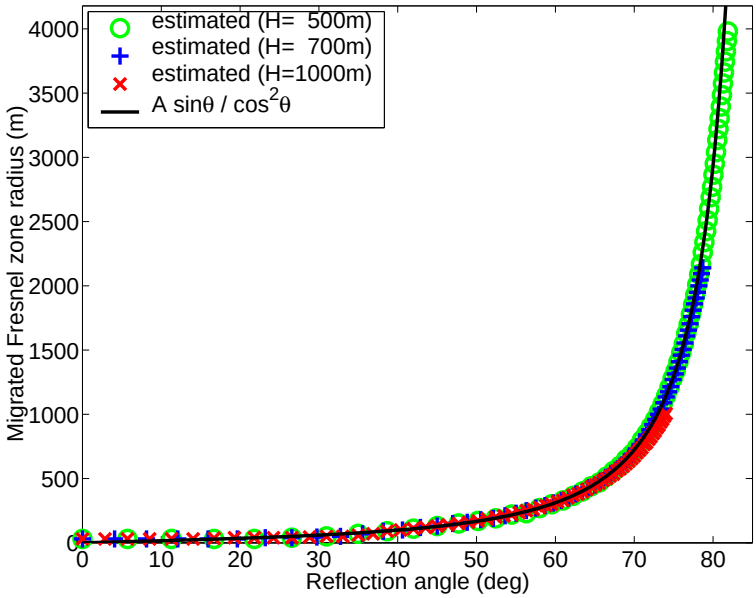


**Figure 9:** Half-axis of the residual transition zone after Kirchhoff depth migration (crosses) for reflectors at depths of 500 m (circles), 700 m (plus signs) and 1000 m (crosses). Also indicated is a fitting curve proportional to $\sin\theta/\cos^2\theta$.

one migrated trace at $x = -500$ m. Its effective wavelet length $z_\varepsilon$ in depth (horizontal bars) is obtained from the effective wavelet length $\tau_\varepsilon$ in time by applying the migration pulse stretch (Tygel et al., 1994), viz.,

$$z_\varepsilon = \frac{v\tau_\varepsilon}{2\cos\beta\cos\theta} \ . \tag{8}$$

Here, $\theta$ is the reflection angle and $\beta$ is the dip angle, i.e., $\beta = 0$ for our example. Also depicted are the two diffraction rays that image points $M$ and $M'$ at the top and the bottom of the effective wavelet length. Considering the wavelet length to be short as compared to the distances to source and receiver, we can assume these two rays to be parallel. Then, the dashed ray reflected at point $M'$ reaches the top of the wavelet at $\overline{M}$ at a distance to $M$ of $r = z_\varepsilon \tan\theta$. Combined with the above expression (8) for the wavelet length in depth, the distance of influence due to a finite pulse length becomes

$$r = \frac{v\tau_\varepsilon \sin\theta}{2\cos^2\theta} \ . \tag{9}$$

In this way, we geometrically obtain a formula for the horizontal resolution that has the same structure as the observed behavior. In particular, it does not depend on depth. Moreover, the direct proportionality to the propagation velocity and the wavelet length has been confirmed by additional experiments. However, when using the same effective wavelet length as before migration, we obtain for the proportionality factor $v\tau_\varepsilon/2 \simeq 55$ m. This seems to suggest that horizontal resolution after migration is governed by a larger effective wavelet length than before migration.

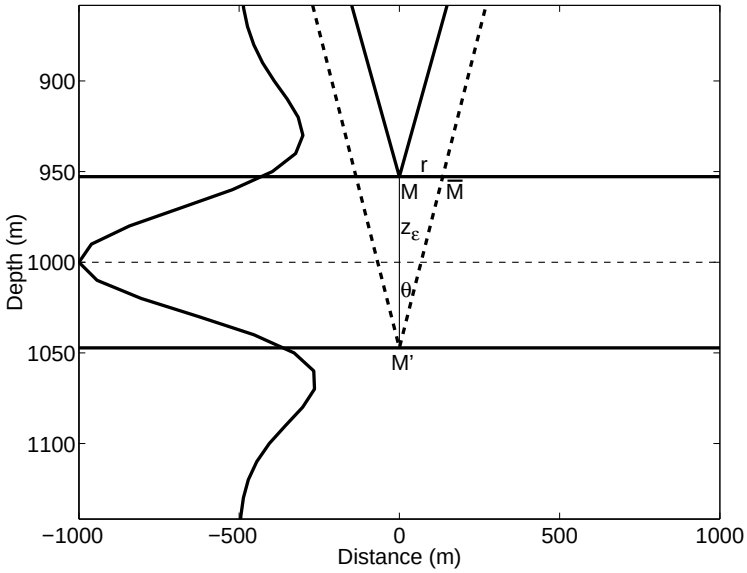


**Figure 10:** Geometrical situation at the reflector image. Shown is the migrated wavelet at $x = -500$ m, together with its effective wavelet length $z_\varepsilon$ in depth (horizontal bars). Also depicted are the two diffraction rays that image the top and the bottom of the effective wavelet length.

### Consequences for AVO/AVA analysis

Above, we have seen that the resolution achieved by Kirchhoff depth migration is strongly angle-dependent. This may influence not only a post-migration stack but also an AVO/AVA analysis. Stacking images of different resolution will, of course, result in a final image that will offer only the lowest resolution achieved in one of the individual images. Therefore, the final stack will exhibit the resolution of the image with the largest offset that was used in the stack.

Concerning AVO/AVA analysis, care has to be taken when analyzing amplitudes close to a strong amplitude variation. The situation is illustrated in Figure 11. The left figure depicts the migrated amplitudes across the vertical fault for several different offsets. Consider an AVO or AVA analysis carried out at the position indicated by the vertical line. As we see, amplitudes are correct at short offsets but incorrect at large offsets. Thus, an AVO analysis would recover a wrong AVO trend.

How this affects the AVO trends at various distances from the fault can be seen on the right-hand side of Figure 11. It depicts the error of the AVO curves as a function of offset. For points relatively close to the fault, the AVO trend is strongly affected, although the amplitudes at the shortest offsets are correctly imaged. The farther from the fault, the better the AVO trend. However, only at very large distances from the fault, the AVO trend is really unaffected by the amplitude variation across it.

## CONCLUDING REMARKS

In this paper, we have discussed horizontal resolution of true-amplitude Kirchhoff depth migration in dependence on the source-receiver offset. By means of the present analysis, we have now gained a much more quantitative understanding of what the common expression “depth migration

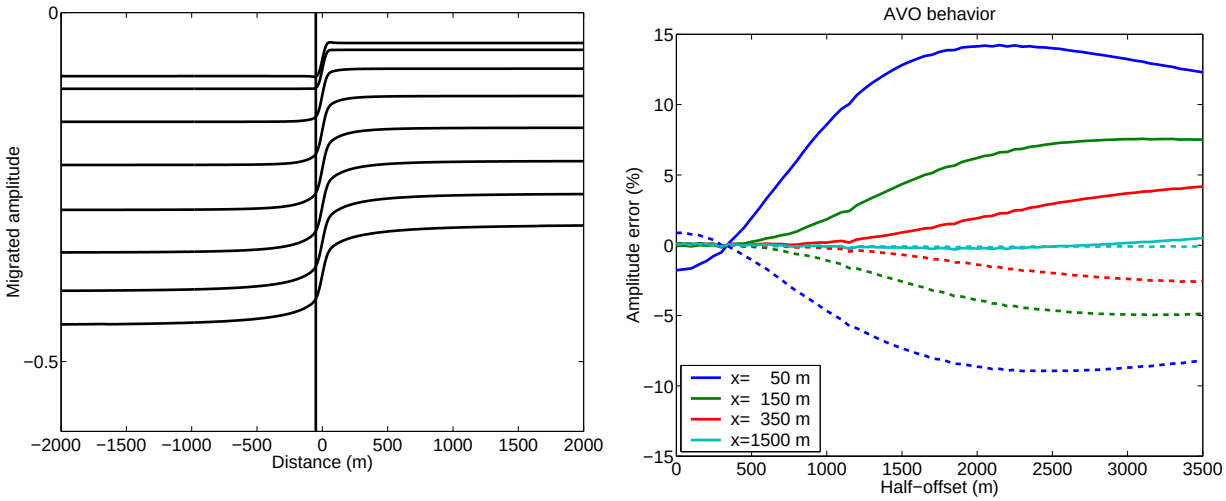


**Figure 11:** Left: Migrated amplitudes at various offsets. Consider an AVO analysis along the position indicated by the vertical line. Right: Errors of AVO trends at different distances from the fault.

reduces the Fresnel zone" means in quantitative terms.

Speaking implicitly in time-domain concepts, the zone of influence around the specular ray changes from the projected Fresnel zone to a residual zone that depends on the length of the seismic wavelet and the reflection angle. For the usual seismic range of offsets and reflector depths, we qualitatively observe the expected behavior of a decreasing horizontal resolving power with increasing offset. However, for very large offsets and shallow reflectors, the resolution after migration may actually even be worse than before.

The quantitative behavior of horizontal resolution as a function of offset is different from that of vertical resolution. As shown by Tygel et al. (1994), for constant velocity and a horizontal reflector, the vertical resolution decreases proportionally to the cosine of the reflection angle. Horizontal resolving power, seems to follow a slightly more complicated function of that angle. The best fitting curve is of the type $r = A \sin\theta / \cos^2\theta$. Geometrical considerations can be found that predict such a behavior. The proportionality factor $A$, however, is not directly explained in this manner.

The observed behavior of seismic resolution after Kirchhoff depth migration must be considered when carrying out an AVO/AVA analysis close to strong amplitude variations. Since amplitudes of images for different offsets may be differently affected by the presence of the amplitude variations, the AVO behavior may be incorrect.

It is to be remarked, that the resolution as described in this paper is reached only with perfect, that is, noise-free, correctly sampled, unbiased data and a sufficiently large migration aperture. Any additional distortion due to the wave propagation in an inhomogeneous reflector overburden, such as transmission losses, focusing and defocusing, caustics, etc., as well as acquisition effects such as irregular source and receiver spacing, source and receiver coupling, uncalibrated traces, small aperture, etc., will not only affect the recovery of the best possible amplitudes but will also degrade the seismic resolution.

## ACKNOWLEDGMENTS

The research of this paper was supported in part by the National Research Council (CNPq – Brazil), the São Paulo State Research Foundation (FAPESP – Brazil), and the sponsors of the WIT Consortium.

## REFERENCES

Berkhout, A. (1982). *Seismic Migration – Imaging of Acoustic Energy by Wave Field Extrapolation*, volume 14A of *Developments in Solid Earth Geophysics*. Elsevier, Amsterdam.

Berkhout, A. (1984). *Seismic Resolution, a Quantitative Analysis of Resolving Power of Acoustical Echo Techniques*. Geophysical Press.

Beylkin, G. (1985a). Imaging of discontinuities in the inverse scattering problem by inversion of a generalized Radon transform. *Journal of Mathematical Physics*, 26(1):99–108.

Bleistein, N. (1987). On the imaging of reflectors in the earth. *Geophysics*, 52(7):931–942.

Cohen, J., Hagin, F., and Bleistein, N. (1986). Three-dimensional Born inversion with an arbitrary reference. *Geophysics*, 51(8):1552–1558.

Gelchinsky, B. (1985). The formulae for the calculation of the Fresnel zones or volumes. *Journal of Geophysics*, 57:33–42.

Hagedoorn, J. (1954). A process of seismic reflection interpretation. *Geophysical Prospecting*, 2(2):85–127.

Hubral, P., Schleicher, J., and Tygel, M. (1992). Three-dimensional paraxial ray properties – Part I. Basic relations. *Journal of Seismic Exploration*, 1(3):265–279.

Kallweit, R. and Wood, L. (1982). The limits of resolution of zero-phase wavelets. *Geophysics*, 47(07):1035–1046.

Knapp, R. (1991). Fresnel zones in the light of broadband data. *Geophysics*, 56(3):354–359.

Schleicher, J. and Santos, L. (2000). Offset-dependent resolution of seismic migration. Annual Report No. 4, WIT Consortium.

Sheriff, R. (1980). Nomogram for Fresnel-zone calculations. *Geophysics*, 45(5):968–972.

Sommerfeld, A. (1964). *Optics*, volume IV of *Lectures on Theoretical Physics*. Academic Press, New York.

Tygel, M., Schleicher, J., and Hubral, P. (1994). Pulse distortion in depth migration. *Geophysics*, 59(10):1561–1569.

Vermeer, G. (1999). Factors affecting spatial resolution. *Geophysics*, 64(3):942–953.